AN APPROACH FOR QUANTIFICATION OF THE HYDRATE RESOURCES USING THE EFFECTIVE MEDIUM THEORY AND AVO ANALYSIS: EXAMPLES FROM THE MAKRAN ACCRETIONARY PRISM, OFFSHORE IRAN

BEHNAM HOSSEINI SHOAR[1], ABDOLRAHIM JAVAHERIAN[1,2], NASSER KESHAVARZ FARAJKHAH[3] and MOJTABA SEDDIGH ARABANI[4]

[1] *Department of Petroleum Engineering, Amirkabir University of Technology, Tehran, Iran.*
[2] *Institute of Geophysics, University of Tehran, Iran. javaheri@ut.ac.ir*
[3] *Exploration and Production Research Center, Research Institute of Petroleum Industry, Tehran, Iran.*
[4] *Department of Geophysics, Exploration Directorate, National Iranian Oil Company, Tehran, Iran.*

(Received July 19, 2013; revised version accepted January 13, 2014)

ABSTRACT

Hosseini Shoar, B., Javaherian, A., Keshavarz Farajkhah, N. and Seddigh Arabani, M., 2014. An approach for quantification of the hydrate resources using the effective medium theory and AVO analysis: Examples from the Makran accretionary prism, offshore Iran. *Journal of Seismic Exploration*, 23: 65-87.

Marine hydrates are globally distributed in deep-sea sediments, such as the Makran accretionary prism, where high operational costs and drilling hazards cause a lack of well data. Although the seismic analyses are efficient methods for detection and delineation of hydrate resources for such unexplored regions, developing a scheme to quantify them would be the ultimate goal. In this study, a quantifying approach is introduced which is called reflectivity template (RT). This approach theoretically calculates normal incident (NI) and Poisson reflectivity (PR) attributes by the effective medium theory (EMT) and creates their intuitive crossplots across a bottom simulating reflector (BSR). By superimposing the attributes derived from amplitude-variation-with-offset (AVO) on RTs, the saturations of the hydrate and free gas near the BSR could be estimated. This technique acts as a quantitative interpretation tool when well log data is not available. It is only needed to make good assumptions about porosity and mineralogical composition of the host sediments. Reliability of this approach was validated by synthetic data and the results showed the RT should be created in a way that it was independent from the velocity ratio assumption. Applying this approach to a 2D marine pre-stack time migrated (PSTM) seismic line have implied geological control over hydrate and free gas saturations in the Makran accretionary prism. Estimated saturations near the BSR were approximately 4-30% for the gas hydrate and 1-7% for the free gas across the seismic line.

KEY WORDS: gas hydrate, BSR, effective medium theory (EMT), AVO analysis, reflectivity template (RT), normal incident reflectivity (NI), Poisson reflectivity (PR)

0963-0651/14/$5.00

INTRODUCTION

Gas hydrates including crystalline solids of water, light hydrocarbon and non-hydrocarbon gases (Hardage and Roberts, 2006) which are spontaneously formed in both permafrost areas and the first few hundred meters below the seafloor of deep marine sediments. The appropriate growth conditions for hydrates are low temperature and high pressure thermodynamic conditions as well as the presence of hydrate forming gases and water (Max et al., 2006). During the past two decades, hydrates have been increasingly the subject of international attention, due to their potentiality as an energy resource for the future (Ruppel, 2007). Consequently, the identification and quantification of gas hydrate in nature is essential in order to evaluate its resource potentiality.

Several seismic techniques continue to be the subject of many investigations to detect, delineate and ultimately characterize the marine gas hydrate resources. The main objective of investigations is to answer exploration geophysicists concerns on primarily where the gas hydrates and free gases are present, and next on where they are commercially accumulated and act as resource potentials. There are some seismic indicators which can answer the first issue. One of them is the well-known bottom simulating reflector (BSR) which appears to be related to the base of the hydrate stability zone. The BSR is resulted from the elastic property contrast through variations in pore-filling substances. It is an interface between upper sediment containing hydrate and lower sediment containing free gas (Hyndman and Spence, 1992; MacKay et al., 1994). Along with the BSR, prospective hydrate resources could be delineated through analyzing other post-stack seismic indicators, such as amplitude blanking (Sinha et al., 2004) and bright spot (Max et al., 2006). Regarding the pre-stack analysis, the amplitude-variation-with-offset (AVO) analysis is an important tool for characterizing conventional hydrocarbon-bearing sands. Foster et al. (2010) analyzed the effect of pore fluid, porosity and lithology on AVO responses. In the case of the hydrate resources, the AVO of the BSR could be used as a hydrate and free gas indicator and provide a qualitative study (Yi et al., 2011; Fohrmann and Pecher, 2012).

On the subject of the quantification of hydrate resources, several seismic analyses have been developed to answer the second issue by appraising hydrate and free gas saturations. The presence of both hydrate and free gases, changes the elastic properties of the host sediments. A small amount of free gas in a pore space dramatically decreases the P-wave velocity (Domenico, 1976) below the BSR. This is while the growth of the hydrates can increase the P- and S-wave velocities above the BSR (Ecker et al., 1998). Different rock physics theories have been developed to analyze and differentiate the elastic property differences of hydrate- and gas-bearing sediments, from those of fully water saturated. The effective medium theory (EMT) is one of the developed theories, which was developed for different hydrate distribution modes (Helgerud et al., 1999). Most

of the hydrate quantification methods use the rock physics theory and translate the elastic properties to saturations where layer's seismic properties are provided (Dai et al., 2004; Lu and McMechan, 2004). Moreover, there are some methods which use the AVO analysis independently (Muller et al., 2007; Ojha and Sain, 2007) or along other methods (Ojha and Sain, 2008) to assess the hydrate and free gas saturations. These methods can render the AVO analysis quantitative.

The present study introduces an approach which combines EMT and AVO methods to model the theoretical intuitive crossplot of BSR's reflectivities. This crossplot is called a Reflectivity Template (RT) and is defined based on normal incident (NI) and Poisson reflectivity (PR) attributes. These attributes are model parameters in Verm and Hilterman's (1995) approximation of Shuey's (1985) equation. By comparing the estimated attributes derived from the AVO analysis of the BSR in the data with those values theoretically calculated in RT modeling, the saturation of gas hydrate and free gas near the BSR could be estimated. To validate an RT approach based on NI and PR, the synthetic common mid-point (CMP) gathers were used. The CMPs were forward modeled based on the exact full elastic wave modeling algorithm assuming a 1D model (no lateral elastic variations). Then, the provided templates were used to appraise a hydrate resource in the Makran accretionary prism, offshore Iran. This area is an un-explored region which contains only sparse 2D seismic lines.

METHODOLOGY

AVO analysis

Zeoppritz's (1919) equations give the exact coefficients for transmission and reflection of a plane wave and its mode converted when an incident at an interface between two semi-infinite isotropic and homogeneous layers happens. The complicated form of these equations makes their inversion algorithm non-linear. Many useful linearized approximations exist which are valid when the relative contrast among the elastic properties across interfaces is small. One of these approximations is Shuey's (1985) relation which decomposes the AVO behavior of an interface to three angle ranges, i.e., normal incidence, intermediate angles, and wide angles. Verm and Hilterman (1995) approximated Shuey's relation with a two-term- equation which is valid when the S- to P-wave velocity ratio (V_S/V_P) is equal to 0.5 and the incidence angle is less than 30 degrees. This approximation decomposes the AVO behavior of a pre-stack reflector into the near offset and far offset reflectivities as follows:

$$RC(\theta) \cong NI\cos^2(\theta) + PR\sin^2(\theta) \quad , \tag{1}$$

where RC is the reflection coefficient and θ is the average of incident and transmitted angles. NI and PR are expressed as

$$NI = (V_{P2}\rho_2 - V_{P1}\rho_1)/(V_{P2}\rho_2 + V_{P1}\rho_1) \ ,$$

and

$$PR = (\sigma_2 - \sigma_1)/(1 - \sigma_{avg}) \ ,$$

where, V_P, ρ and σ are P-wave velocity, density, and Poisson's ratio, respectively. For a reflector in the pre-stack data, eq. (1) can be written as

$$\begin{bmatrix} RC(\theta_1) \\ . \\ . \\ . \\ RC(\theta_n) \end{bmatrix} = \begin{bmatrix} \cos^2\theta_1 & \sin^2\theta_1 \\ . & . \\ . & . \\ . & . \\ \cos^2\theta_n & \sin^2\theta_n \end{bmatrix} \begin{bmatrix} NI \\ PR \end{bmatrix} \text{ or } d = Gm, \qquad (2)$$

where, m is the model parameter matrix, G is the angle dependent matrix and d is the angle dependent reflection coefficient matrix. In addition to the direct solution from angle stacks, making inference about the model parameters (m) from the amplitude data (d) was provided by a solution of a set of linear equations. In other words, regarding eq. (2), at each time sample the NI and PR AVO attributes are the model parameters and extracted from amplitudes of different offsets in a common depth point (CDP) gather. This requires knowledge of incidence angle function of offset and time, which could be approximated by knowing the velocity information. The least squares and the robust are two commonly used solutions for a set of linear equations. The least squares solution of the linear inverse problem is expressed as follows (Sen, 2006):

$$m = (G^TG)^{-1}(G^Td) \ , \qquad (3)$$

where T denotes the matrix transpose. The main disadvantage of this method is its sensitivity to uncharacteristic amplitudes which are known as outliers. The robust method can accommodate outliers and works by weighting amplitude data points automatically and iteratively (Walden, 1991). In the first iteration of the robust method, the same weight is assigned to each point and model parameters are estimated using ordinary least squares. At subsequent iterations, weights are recomputed. Lower weights are given to the points farther from the model predictions in the previous iteration. The model parameters are then recomputed using weighted least squares. Therefore, this method minimizes the influence of the outliers.

Effective medium theory (EMT)

If the sediments are considered as randomly packed spheres, gas hydrate can grow within the porous media in four identifiable micro modes, here called Modes 1 to 4 (Fig. 1). In Mode 1, or the pore-filling mode, hydrates float in the pore space, do not touch the sediment grains, thus they only change the bulk modulus of the pore fluid. This mode of hydrate distribution has the slightest effect on the host sediment elastic properties. In Mode 2, or the matrix support mode, hydrates are treated as a part of the grains without any cementing effect, and reduce the sediment porosity. In Mode 3, or the contact cementing mode, the hydrates cement the grains at their contact surfaces and dramatically increase the sediments stiffness. In Mode 4, or the grain coating mode, hydrates grow around the grains and reinforce the sediments. These modes are discussed in detail by Ecker et al. (1998). Each hydrate distribution mode has an exclusive effect on the elastic properties. Hereupon, the change in the elastic properties, as a consequence in the value of reflection coefficient of the BSR, depends not only on the saturation of the gas hydrate and free gas, but also on the distribution modes of the hydrate in the host sediments. An improved understanding of the hydrate distribution mode provides a better understanding of the seismic response from the hydrate resources.

There are various rock physics translators of elastic properties to hydrate saturation and vice versa, which are important for rock physics inversion and forward modeling, respectively. The EMT is the proposed method for calculation of elastic properties of the unconsolidated and high-porosity hydrate-bearing sediments. This method is developed for four modes of hydrate distribution (Fig. 1). It has been applied to both non-cementing (Dvorkin and Nur, 1996) and cementing (Dvorkin and Nur, 1993) hydrate distribution modes. A non-cementing approach initiates with computing the elastic moduli of a dry sediment frame at a critical porosity using Hertz-Mindlin contact theory (Mindlin, 1949). Subsequently, the bulk and shear moduli of the dry frame are

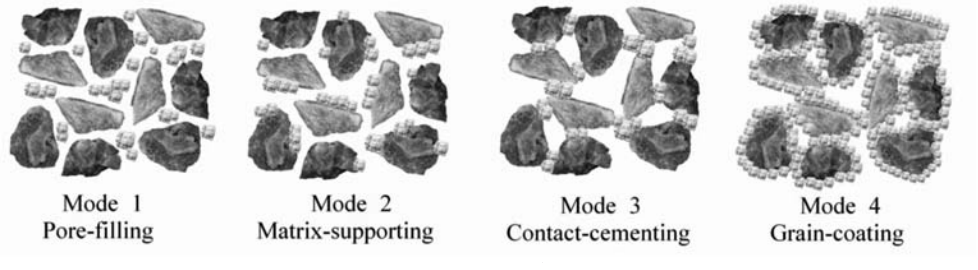

Fig. 1. Classification of the hydrate distribution modes in EMT. Modes 1 and 2 are known as non-cementing modes and Modes 3 and 4 are known as cementing ones. Ecker et al. (1998) describe a detailed calculation procedure for elastic properties of non-cementing and cementing modes.

calculated for porosities above and below the critical porosity, using modified Hashin-Shtrikman (1963) upper and lower bound, respectively. The hydrate-saturated sediment moduli are then calculated using Gassmann's (1951) equation (appropriate for the seismic frequency). For the cementing approach, the dry sediments moduli, cemented by the hydrate, are calculated using the cementation theory (Dvorkin and Nur, 1993). The saturated rock properties are again calculated using Gassmann's equation. These theories are discussed in detail by Ecker et al. (1998). Also, by considering the homogeneous saturation of the free gas below the BSR, Gassmann's equation can be applied to calculate the elastic properties of the free gas saturated sediment. The key elements for deriving the elastic properties based on EMT theory are good assumptions about the mineralogical constituents, porosity, and average of the grain contact numbers. Table 1 lists the elastic properties of the mineralogical constituents considered in this research.

Table 1. Elastic properties of different constituents used for EMT rock physics modeling.

Components	Bulk modulus (GPa)	Shear modulus (GPa)	Density (g/cm^3)	P-wave velocity (m/s)	S-wave velocity (m/s)	References
Calcite	76.8	32.0	2.71	6639	3436	Sloan, 1998
Clay	20.9	6.85	2.58	3412	1629	Helgerud et al., 1999
Quartz	36	45	2.65	6018	4121	Helgerud et al., 1999
Hydrate	6.41	2.54	0.91	3281	1670	Sloan, 1998
Sea water	2.49	0	1.03	1554	0	
Gas (methane)	0.11	0	0.23	691	0	Helgerud et al., 1999

Reflectivity template

The reflectivity templates (RT) are intuitive crossplots of the different AVO attributes that are defined in different linearized approximations. These AVO attributes are usually the relative property contrasts across the BSR which can be expressed as reflectivities. Fig. 2 depicts a schematic sketch of the BSR interface which cross-cuts the stratigraphic reflectors. Consequently there are no changes in the sedimentological properties and lithology of the host sediments just in the BSR vicinity in most of the cases. In other words, the BSR contrast is assumed to be a result of variation in pore-filling substances. Therefore, the host sediment properties could be identical above and below this interface and the variation of the AVO attributes could be given to the effects of hydrate and free gas; these attribute values are controlled by the amount of the hydrate and

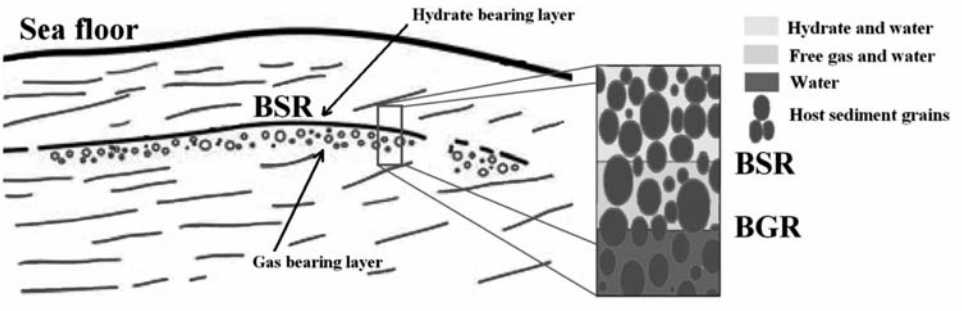

Fig. 2. Cross cutting nature of the BSR. The host sediment properties could be considered identical across this interface where the BSR cuts diagonally through the reflections from strata. Therefore, the variation of the AVO reflectivities could be attributed to the pore-filling substances effects.

free gas and the distribution modes. This BSR characteristic is the basis of the RT approach. The RT can be modeled in different ways, using intercept and gradient attributes (based on Wiggins et al., 1983), or P- and S-impedance reflectivities (based on Fatti et al., 1994). In this study, the RTs are modeled based on NI and PR attributes which are defined in eq. (1), in which the NI is the acoustic impedance reflectivity. However, PR is not a reflectivity as commonly defined by geophysicists; it is convenient to refer to it as the Poisson reflectivity.

The RT approach simply collates NI and PR attributes estimated from the BSR's AVO behavior with those values theoretically calculated by the EMT for several hydrate and free gas saturations and considering different hydrate distribution modes. Parameters used in the EMT should be constrained by a reasonable assumption about the geology and compactional trend by assuming the porosity, mineralogical constituents and average grain contact number. An increase in the compaction and depth decreases the porosity while it increases the grain contact number. For unexplored regions, there are some relations for estimation of porosity and the average grain contact number. This relation can be used to constrain rock physics modeling in these regions. Regarding the mineralogical constituents, the average background constituents in the region can be assumed. These parameters, are site-specific and depending on the local geological situation, are kept constant for each RT; only the free gas saturation (S_g), the hydrate saturation (S_h), and the distribution mode of the hydrate are allowed to change.

RT based on NI and PR^{EMT}

This study had begun by modeling of RT based on the BSR's NI (x-axis) and PR (y-axis) attributes defined in Equation (1). The modeling steps for this RT are; (1) assuming reasonable parameters for the host sediment, (2) calculating the elastic properties of hydrate and gas bearing sediments for several saturation values, (3) calculating the NI and PR attributes for BSR according to Equation (1) and finally, (4) crossplotting of the calculated attributes. Because the PR attribute in this RT is calculated only based on the EMT, its symbol was superscripted by the EMT and denoted by PR^{EMT}.

Fig. 3 shows the RT of NI-PR^{EMT} for four hydrate distribution modes. Assumed mineralogical constituents, porosity, and average grain contact number are shown in Table 2. They are assumed to be identical across the BSR for hydrate and gas-bearing sediments. The saturation values of the hydrate above

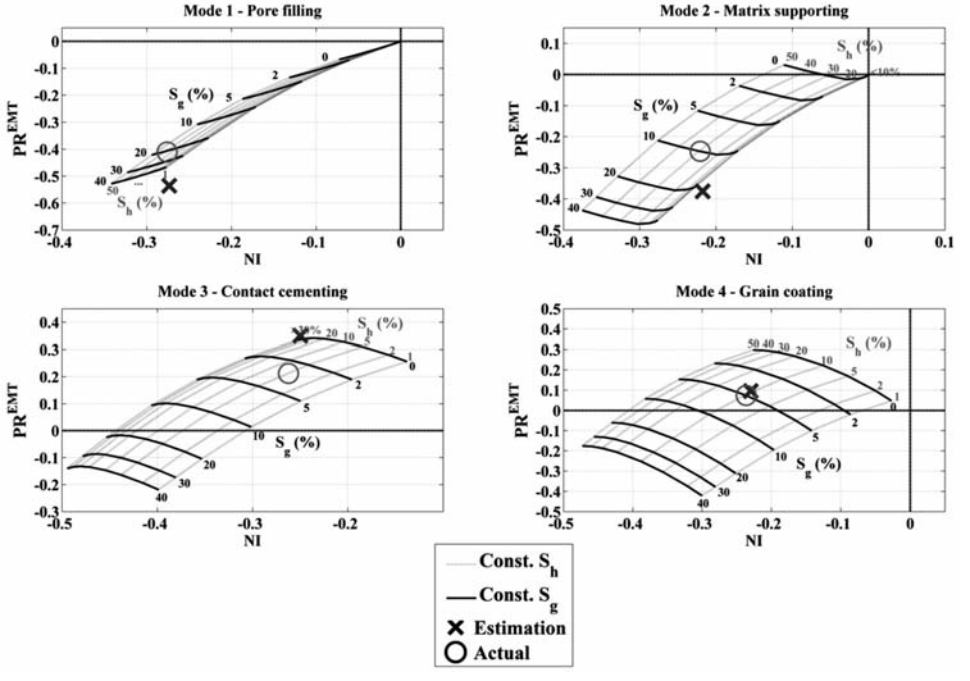

Fig. 3. The RT based on NI and PR^{EMT} for four possible hydrate-distribution modes. Sedimentological properties in Table 2 were used for calculations. The solid dark lines show the constant gas saturation, while the gray dash ones show the constant hydrate saturation. The circle markers and cross markers show the actual and estimated positions for the synthetic data examples, respectively. As it might be expected, a substantial deviation exists along the PR^{EMT} axis which implies that the error in estimation of PR is more significant than in NI.

Table 2. Parameters used for the RT modeling and the synthetic data examples.

	Parameters	Values
Sedimentological	Quartz percent	80%
	Clay percent	20%
	Average grain contact number, n	8
	Sediment porosity	45%
	Critical porosity, ϕ_0	36%
Geometrical	Water depth	1300 m
	BSR depth	1650 m
	BGR depth	1850 m

the BSR are 1%, 2%, 5% and 10 to 50% at 10% intervals. The saturation values of the free gas below the BSR are 0%, 2%, 5% and 10 to 40% at 10% intervals. Several observations can be considered from the analysis of RTs in Fig. 3 including: (1) an increase in the hydrate and/or the free gas saturation renders the NI value of the BSR more negative. This causes the negative amplitude of BSR to appear more clearly on the near normal incidence seismic section. In this regard, the effect of the gas saturation is more considerable than the hydrate saturation. (2) The PR values of the BSR are very sensitive to the hydrate distribution modes and controlled by the saturation of the both hydrate and free gas. (3) The dependency of PR values to the gas saturation variation is pronounced more than the hydrate saturation. (4) The variation of PR values with hydrate saturation is small in non-cementing hydrate distribution modes compared to the cementing ones. It is implied that the non-cementing hydrate has a smaller effect on Poisson's ratio with respect to the cementing mode. (5) For the non-cementing hydrate, the value of PR is mostly negative, while for cementing mode, the value of PR could be both negative and positive.

RT based on NI and PR^{AVA}

As usually defined in linearized approximations, S- to P-wave velocity ratio (V_S/V_P) is the average value across an interface. In addition to the small property contrasts and low incidence angle, another assumption in eq. (1) is the velocity ratio which is assumed to be 0.5. Violation from this assumption imposes erroneous AVO analysis results using eq. (1). This is while hydrates usually form within young and unconsolidated sediments in marine environments where the mentioned ratio is lesser. Moreover, the presence of both hydrate and free gas near the BSR violates this assumption by changing the elastic

properties. Fig. 4 shows the variation of V_S/V_P with the saturation of both hydrate and free gas for four different hydrate distribution modes. Its value increases with an increase in gas saturation. It is while the changes of V_S/V_P with hydrate saturation, are depending on hydrate distribution modes. For Mode 1, V_S/V_P decreases with increasing hydrate saturation, due to an increase in V_P when the V_S remains almost unaffected. For Mode 2, V_S/V_P stays almost flat in low hydrate saturation, while in high hydrate saturation it is increased due to the effect of porosity reduction in a dramatic increase of S-wave velocity. For Modes 3 and 4, the cementing and stiffening effect of hydrate increases V_S/V_P as well as its variation in comparison with Modes 1 and 2.

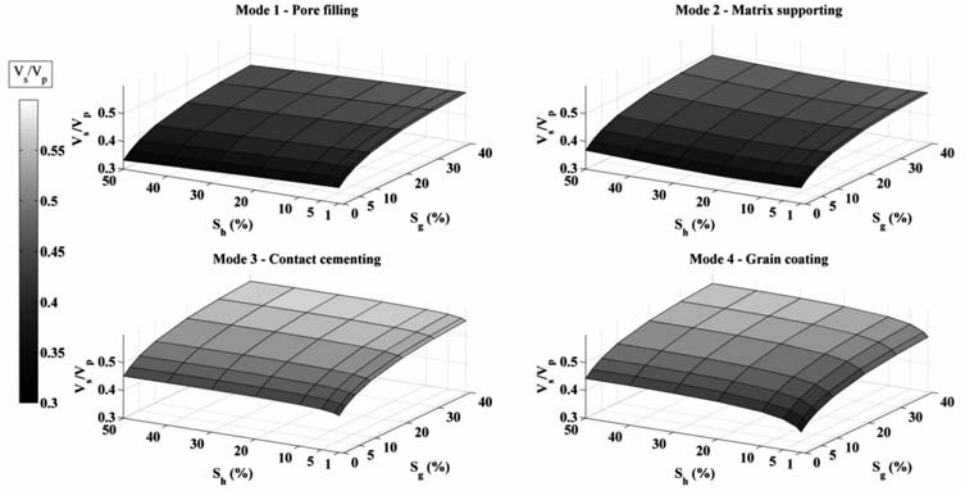

Fig. 4. Variation of V_S/V_P (average values of hydrate- and gas-bearing sediments) across the BSR with saturation of hydrate and free gas. The sedimentological properties of host sediments are listed in Table 2. Note to the V_S/V_P value for the hydrate saturation of 10% and gas saturation of 5% in Mode 4.

Hence, for more reliable quantification by solving the problem of velocity ratio assumption, two steps are added in the RT modeling. The modeling steps for this RT are: (1) Assuming reasonable parameters for host sediment. (2) Calculating the elastic properties of hydrate and gas bearing sediments for several saturation values. (3) Forward modeling of BSR's amplitude-variation-with-angle (AVA) behavior by Zoeppritz's (1919) equations. (4) Inverting the modeled AVA behavior to derive NI and PR attributes by Equation (1) and (5) crossplotting of calculated attributes. Because the PR attribute in this RT was

estimated based on the AVA inversion of the modeled BSR, its symbol was superscripted by AVA and denoted by PR^{AVA}. Fig. 5 shows the RT of NI-PR^{AVA} for the four hydrate distribution modes. The sedimentological information is identical to those listed in Table 2.

Comparing Figs. 3 and 5 for the constant hydrate and gas saturation lines implied that: (1) Their NI attributes are the same in both RTs, as the result of the independency to the velocity ratio assumption. (2) The dependency of PR^{EMT} attribute to the gas saturation variation is slightly more pronounced than that of PR^{AVA} attribute (especially for modes 2, 3 and 4). (3) The dependency of PR^{AVA} attribute to the hydrate saturation is more pronounced than that of PR^{EMT} attribute; this provides an easy quantification of hydrate saturation using PR^{AVA}-NI RTs with respect to the PR^{EMT}-NI RTs.

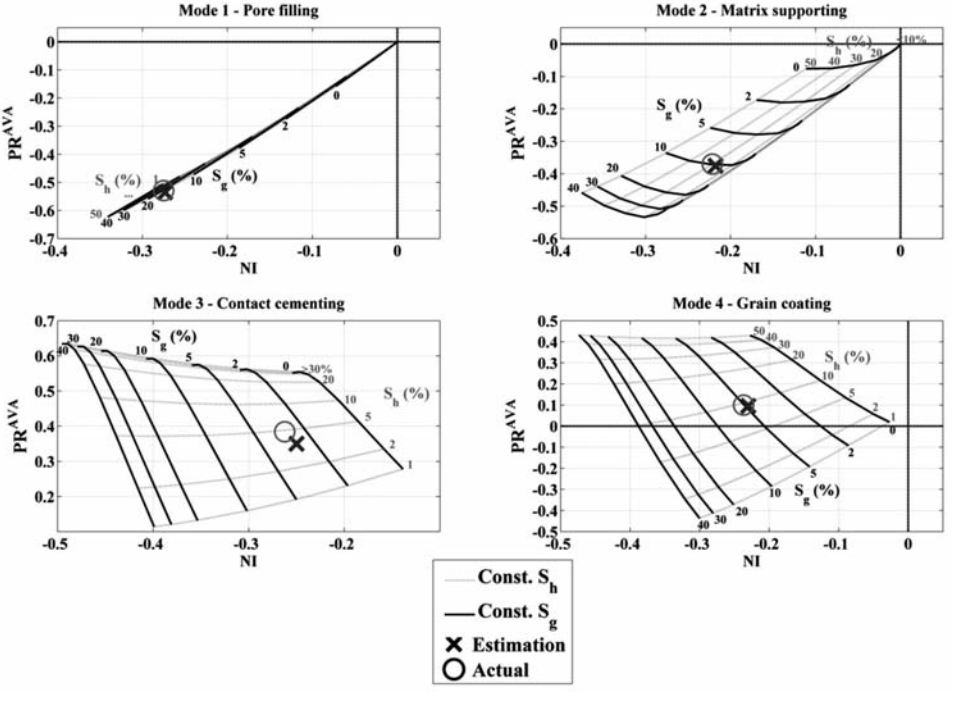

Fig. 5. The RT based on NI and PR^{AVA} for four possible hydrate-distribution modes. All parameters for the calculation are identical to the ones in Fig. 3. The differences between this figure and Fig. 3 are in their modeling steps which are described in the text. There is a minor deviation of the estimated positions (cross markers) from the actual ones (circle markers). Note the synthetic model, a representative of Mode 4, which shows good estimation results in both RTs (see text and Fig. 4 for the reason).

EXAMPLES

Synthetic data

To assess the reliability of RT approach and substantiating its application in quantitative gas hydrate studies, synthetic data representative of four different modes of hydrate distribution were considered. The data were CMP records of four horizontal layers including the water column, hydrate bearing, gas bearing, and fully water saturated layers. All the layers in these models had identical host sedimentological properties. The parameters used in the synthetic data forward modeling are listed in Table 2. The saturations of the hydrate-gas in the four representative models were 40%-20%, 30%-10%, 5%-3% and 10%-5% for Modes 1, 2, 3 and 4, respectively. In these models the selected saturation values of the hydrate and free gas do not produce elastic property contrasts that violate small contrast assumption of linearized approximations. The accuracy of the linearized attributes would be reduced for models in which the high values of hydrate and free gas saturations produce huge contrasts. Fig. 6 shows the forward modeling and AVO analysis procedures for the representative model of Mode 2 where the saturations of hydrate and gas were 30% and 10%, respectively. The EMT, rock physics modeling of unconsolidated sediments, was used to determine the elastic properties. The background elastic properties were calculated by assuming fully water-saturated sediment. Note the variation of elastic properties due to the presence of hydrate and free gas which are shown in Fig. 6a. Using an approach based on an exact elastic wave algorithm (Kennett, 1983), synthetic CMP records were generated. This algorithm simulates seismic wave propagation in a 1D stratified earth model. This type of the earth model can be expressed in a series of layers that are internally homogeneous. Because of a large offset with respect to the target depth, the non-hyperbolic normal moveout (NMO) correction was applied. The NMO corrected CMP record is shown in Fig. 6b. After estimating the incidence angles based on smoothed velocity model, the AVO attributes, NI and PR, were estimated by the least squares solution (eq. (3)) for each time sample. The results of the derived attributes are shown in Fig. 6c.

After estimating the AVO attributes of the BSR for four representative models, their values were picked, superimposed to the related RT, and compared with their actual positions. The results of mapping the NI and PR values of each model to the RT of NI-PR^{EMT} and RT of NI-PR^{AVA} are shown in Figs. 3 and 5, respectively. In both figures, the actual positions of the synthetic models are shown by circle markers and the results of superimposing their estimated reflectivities by the AVO analysis are shown by cross markers. Regarding the RT of NI-PR^{EMT}, the estimated attributes show a substantial deviation from the expected positions (Fig. 3). This could be mainly due to a violation of assuming $V_S/V_P = 0.5$. These deviations impose an erroneous prediction of hydrate and gas saturations using the RT of NI-PR^{EMT}. There is an

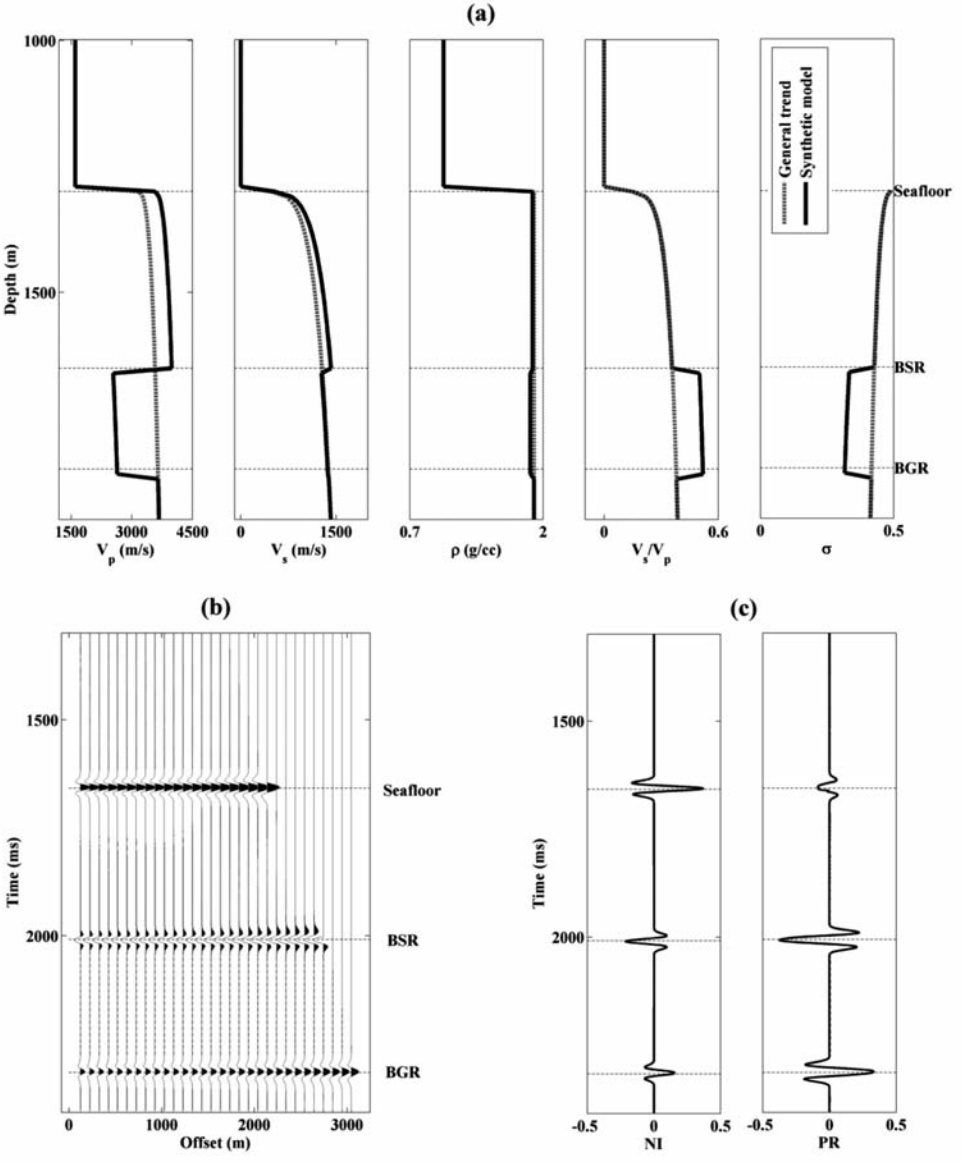

Fig. 6. Synthetic data example for the model in which the saturations of hydrate and gas were 30% and 10%, respectively and the hydrate distribution was Mode 2. (a) The results of elastic properties forward modeling using EMT. The dark solid lines correspond to the model's properties while the gray dash lines are the wet (fully water saturated) host sediment's elastic properties. The elastic properties change dramatically across the BSR and the bottom of gas reflector (BGR). (b) The synthetic seismogram which is a CMP record after the NMO correction, and a muting which consists of 120 traces at offsets with a 50 m interval (every fourth trace is shown in the display). (c) AVO-derived attributes: NI and PR traces.

exception in the grain coating model in which the deviation is small. It is because the V_S/V_P is close to 0.5 (see saturation of 10% for S_h and 5% for S_g in grain coating mode in Fig. 4). On the other hand, there are good agreements between the estimated attributes and the expected positions when using the RT of NI-PR^{AVA} (Fig. 5). There are only minor deviations of the actual values from the estimated ones due to an error in the estimation of incidence angles. Accordingly, the RT of NI-PR^{AVA} can predict the hydrate and gas saturations more precisely than RT of NI-PR^{EMT}.

Field data in the Makran accretionary prism

For field data example of hydrate resource, one of the 2D lines in the Iranian part of the Makran accretionary prism was considered. This area of study is an unexplored region, with no wells drilled in the offshore area. The occurrence of hydrate in deep sea sediment in this area has been verified through a qualitative study based on the presence of BSRs and other seismic indicators (Hosseini Shoar et al., 2009). However, this area has not been subject of gas hydrate quantification studies before. In selected 2D line for an RT-quantification study, the streamer consisted of 480 hydrophone groups, with a 12.5 m group interval located at a depth of 6 m with a shot interval of 25 m. These acquisition parameters yielded 120 traces in each CMP gather. The reprocessing was performed in a way that the relative amplitudes were not

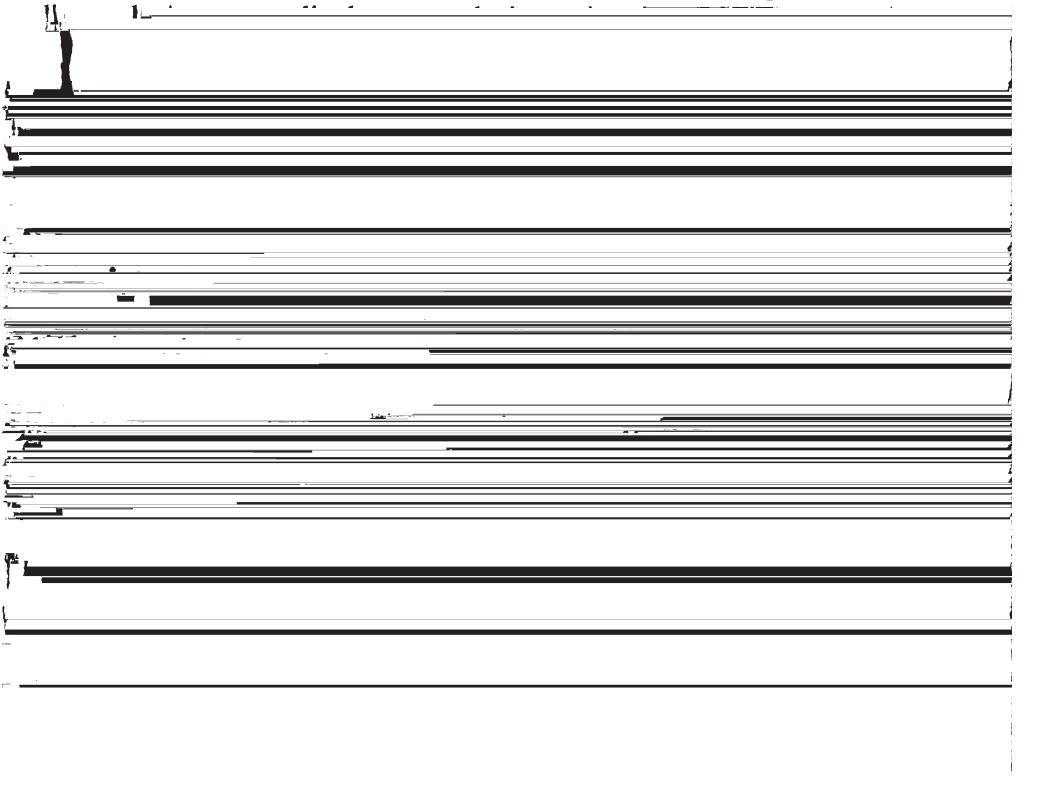

reflectors, horizon-based trim statics was applied based on six picked horizons (including the BSR) on the PSTM section.

3. To estimate the incidence angles for each offset and time sample, a good velocity model was required. The PSTM root-mean-square velocity was converted to the interval velocity and used for incidence angle estimation.

Fig. 7 shows the PSTM section of the selected line between CRPs 11700 to 13400. There is a strong BSR at about 2450 to 2700 ms TWT on different structural features. The thrusted-ridge type of the BSR was developed within the compressional structures on top of the thrust fault hanging-wall. In this structure, formation of an appropriate closure for the accumulation of free gas beneath the BSR is expected. In contrast, the thrusted-footwall type of BSR appeared in the footwall strata of the thrust fault. The basin-margin type of the BSR was formed along the margin of the slope basin on the hanging wall of thrusts (Lin et al., 2009). Fig. 8 displays five representative CRP gathers 11932, 12245, 12485, 12812 and 13298 (top row), the BSR's AVA behavior (middle row) and the crossplot of intercept along with the gradient values (bottom row). The short wavelength or trace-to-trace variations of the amplitudes in the middle row are assumed to be due to the noise or interfering of a crosscutting BSR with other reflections. The AVA responses of the BSR in this CRP were categorized into two classes: (1) Class III in which the BSR

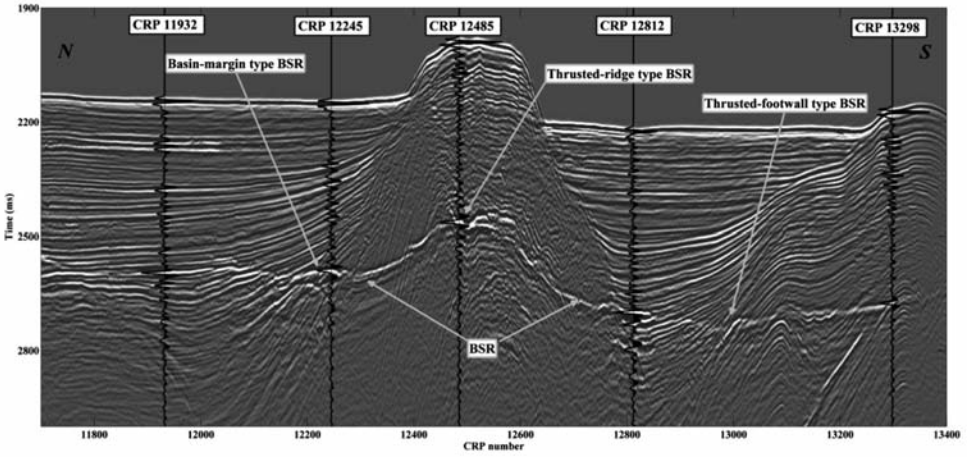

Fig. 7. A seismic section along the North-South seismic line in the Makran accretionary prism showing the BSR types of thrusted-ridge, thrusted-footwall and basin-margin. Individual wiggle traces illustrate the positions of the representative CRP gathers for the RT analysis.

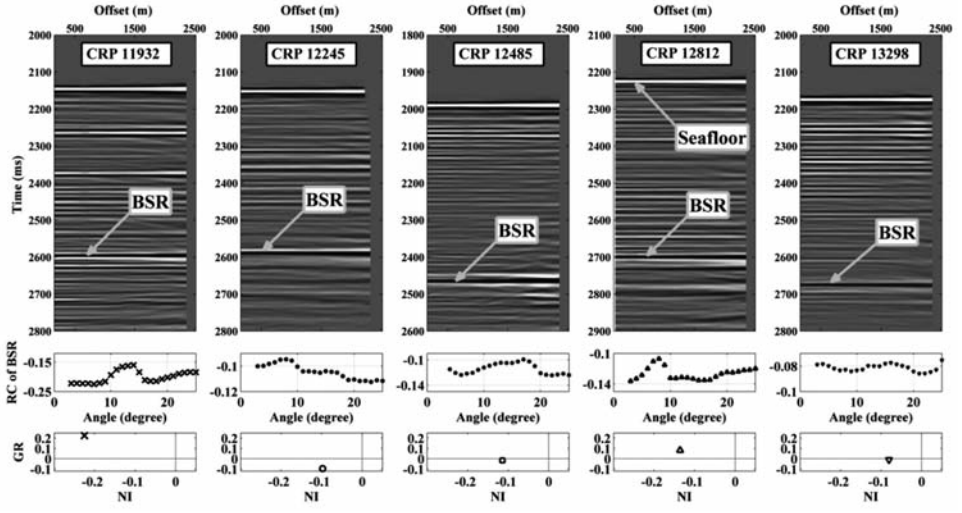

Fig. 8. Five representative CRP gathers (top row) and their AVA (middle row) as well as a crossplot of their NI and GR values (bottom row) for the BSR. The BSR's AVA behavior and its NI-GR values show the AVO class III for CRPs 12245, 12485 and 13298 and the AVO class IV for CRP 11932 and 12812. Their AVO classes are applicable for selection of the proper RT based on the hydrate distribution modes. The positions of the CRPs on seismic section are shown in Fig. 7. GR denotes the gradient.

had a large negative reflection coefficient at zero incidence angle (R0) and became more negative in a further offset; note the AVA behaviors of CRPs 12245, 12485 and 13298. (2) Class IV in which the negative R0 became less negative with the offset; see the AVA behaviors of CRPs 11932 and 12812. The AVA behavior could be attributed to the effect of the hydrate on the sediment S-wave velocity (Castagna et al., 1998). For cementing modes, the hydrates cement the grains and increase the S-wave velocity above the BSR, thus producing an AVO class IV, whereas non-cementing hydrates do not alter the S-wave velocity significantly and produce an AVO class III due to the presence of gas below the BSR. These AVO responses were used for selection of a proper RT based on the hydrate distribution modes. Therefore, the RT of cementing modes for CRPs 11932 and 12812 and the RT of non-cementing modes for CRPs 12245, 12485 and 13298 could be considered for quantification.

For an AVO analysis, the amplitude data up to a maximum angle of 25° were used to estimate the model parameters, NI and PR, in eq. (1). In addition to applying a trim static in the preconditioning step, a tracker was used to follow reflectors in gathers. Because of the interfering nature of the BSR, the

robust estimation method was used for the AVO attributes estimation, which greatly limited the effects of outlying amplitudes.

For a quantitative analysis, NI and PR values of the BSR for five representative CRPs were picked and superimposed on a suitable RT of NI-PR^{AVA} provided based on the parameters listed in Table 3. The references to the parameter selection were previous gas-hydrate studies in the Makran area (Sain et al. 2000; Fowler et al., 1985; Minshull and White, 1989) and relations from Athy (1930) and Murphy (1982). Fig. 9a shows the seismic section with interpreted faults. A series of high amplitude dipping reflectors beneath BSRs can be found in the thruted-footwall and basin margin types of BSR structures. The amplitude of these reflectors weakened above the BSR. This reduction in the amplitude of stratigraphic reflections is known as amplitude blanking. Fig. 9b shows the non-cementing RT of Mode 2 with mapped estimated values of NI and PR for the BSRs in CRPs 12245, 12485 and 13298 which indicated an AVO class III for the BSR. The results showed the hydrate and gas saturations of about $<10\%$ and 3% around CRP 12245, 30% and 1% around CRP 12485, and 25% and 1% around CRP 13298. Fig. 9c shows the cementing RT of Mode 4 as well as superimposed values of NI and PR for CRPs 11932 and 12812 that showed an AVO class IV for the BSR. The results indicated hydrate saturations of about 8% and 4% and gas saturations of about of 7% and 4% at CRPs 11932 and 12812, respectively.

Table 3. Parameters for the rock physics modeling of the unconsolidated sediments in the Makran area.

Parameters	Value or relation	References
Quartz percent	80%	Sain et al., 2000
Clay percent	20%	Sain et al., 2000
Sediment depth, Z	410 m	Observed BSR on the seismic section
Seafloor porosity, ϕ_0	60%	Fowler et al., 1985
Sediment porosity	$\phi = \phi_0 e^{-(Z/\lambda)} \approx 42\%$	Athy, 1930
Compaction constant, λ	1.17	Minshull and White, 1989
Critical porosity, ϕ_0	36%	Dai et al., 2004
Number of contacts per grain	$n = 20\text{-}34\phi + 14\phi^2 \approx 8$	Murphy, 1982

There are several correlations between the estimated saturations and geological features in the hydrate resource prospect in this study. The estimated saturations of free gas in different locations indicated that they accumulated

preferably beneath the crosscutting BSR in basin-margin and thrusted-footwall structures. This effect may exist because when free gas tends to migrate upward toward structural high, it gets trapped below hydrate bearing strata. The presence of the amplitude blanking in the stacked seismic section could demonstrate these features. Also, it is usually expected that the BSR within a compressional structures such as thrusted-ridge, produces an appropriate location for the accumulation of the free gas. In other words, the presence of higher saturations of gas below the BSR with good closure is usually anticipated in the crest of this type of structure. However, the estimation results show lower gas saturation in the thrusted-ridge structure compared to the free gas accumulated beneath the surrounding BSR. It was speculated that the presence of normal faults on top of the thrust faults (interpreted in the seismic section in Fig. 9a) was the probable cause of the low gas saturation. These faults may act as conduits and facilitate the migration of free gas to hydrate stability zone (above BSR), and may cause the richness of hydrate (for example, hydrate saturation about 30% in CRP 12485) in the crest of thrust hanging-wall.

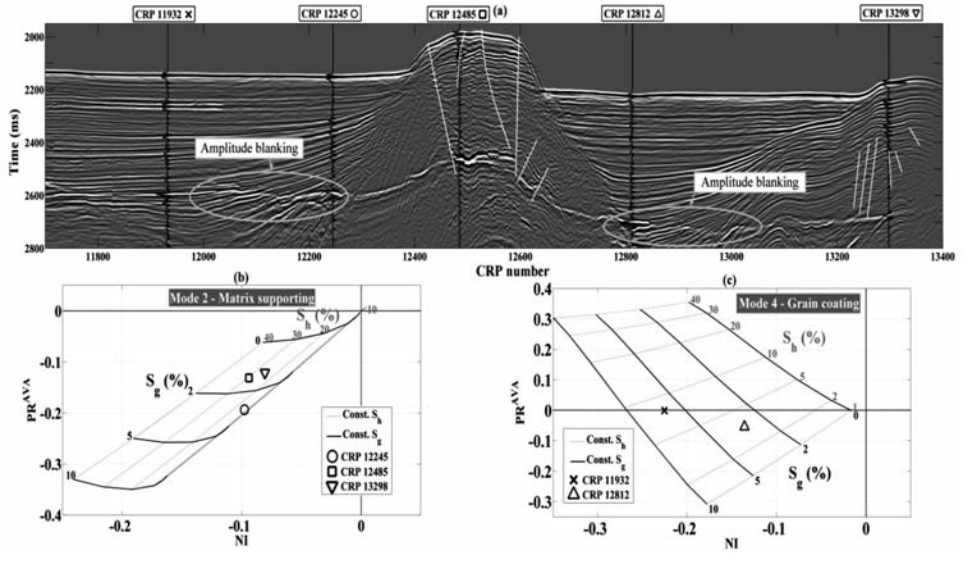

Fig. 9. (a) Interpreted faults as well as amplitude blanking indicators on seismic section used for correlating estimated hydrate and free gas saturations with geological evidences. (b) Quantification of the hydrate and free gas close to the BSR in CRPs 12245, 12485 and 13298 using the RT of Mode 2. The superimposition of NI and PR values shows the hydrate saturation of < 10%, 30% and 25% and gas saturation of 3%, 1% and 1% in the positions of CRP 12245, 12485 and 13298 respectively. (c) Quantification of the hydrate and free gas close to the BSR in CRPs 11932 and 12812 using the RT of Mode 4. Superimposing the estimated values of the NI and PR on the RT shows the hydrate saturation of 8 and 4% and gas saturation of 7 and 4% in the positions of CRPs 11932 and 12812, respectively.

DISCUSSION

By combining gas hydrate rock physics modeling based on the EMT and

fluid variations, mineralogical changes have a negligible effect. Regarding the AVO analysis, the ambiguities associated with the estimation of NI is small compared to the estimation of PR. In practice, the RT approach will be beneficiary of a way that improves the AVO-derived attributes. Using a 3D AVO analysis instead of the 2D one or even an improvement in the estimation of incidence angle by the available velocity model should be helpful for this purpose. Moreover, the final source of uncertainty is the tuning of the BSR with other reflections and the noise in the seismic data. Using a robust estimation method for model parameter estimation, suppressed the effect of the outlying or uncharacteristic amplitudes mainly resulted from the interference of the reflectors and the presence of noise. The difference between the results of the least squares method and the robust method is shown in Fig. 11. It could be seen that the difference is substantial and it reflects the dependence of the AVO attributes estimation results on the used method. In this figure, the robust method considerably suppressed the effect of the large amplitude value in low angles. The values of root-mean-squared error (RMSE) for both methods verify the robust effectiveness.

Generally, in unexplored areas covered with only seismic data with no existing well information, utilizing the RT approach, beside all associate uncertainties, can draw additional insight in selecting a potential prospect for further studies.

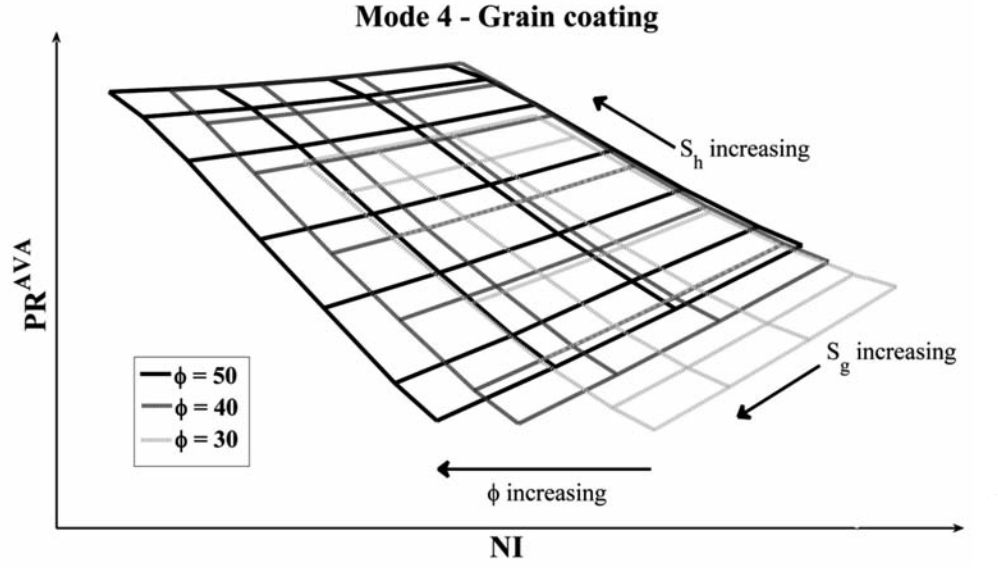

Fig. 10. The schematic NI-PR^{AVA} RTs of Mode 4 calculated for three different porosity values (see text for description).

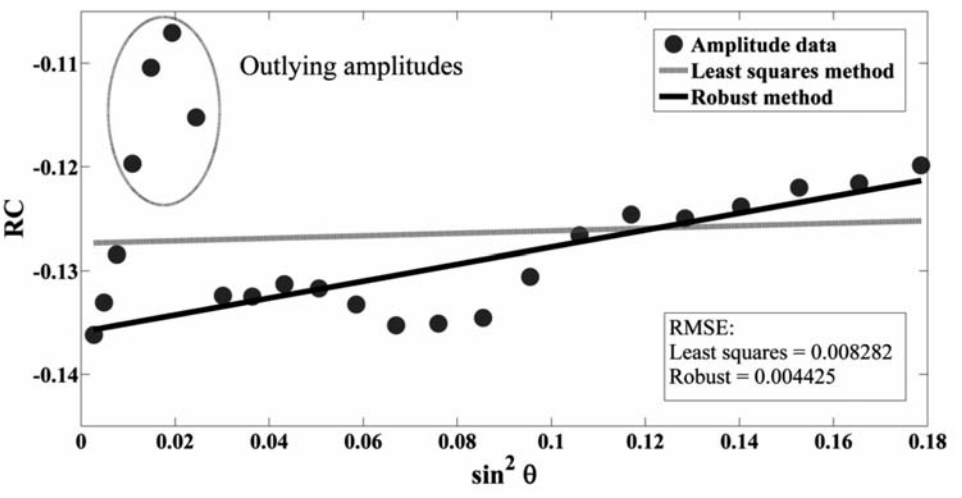

Fig. 11. Demonstration of the difference between the ordinary least squares method and the robust method for estimation of intercept and gradient attributes of the BSR in CRP 12812 shown in Fig. 8. It displays a scatter plot of $\sin^2\theta$ and amplitude values, fitted lines by least squares and robust methods plus an estimate of the root mean squared error (RMSE) from both. RC is roughly a linear function of $\sin^2\theta$. However, a few points are outliers (they fall far from the trend) which could be the result of the cross cutting nature of the BSR or the presence of the noise.

CONCLUSIONS

The approach introduced in this paper was based on the theoretical intuitive crossplots of properly computed NI and PR of the BSR. These crossplots were calculated for four different hydrate distribution modes and called reflectivity template (RT). They were used to estimate the hydrate and gas saturations using the AVO analysis of the distinguishable BSR. Applying the RT approach for synthetic data implied that the estimation accuracy of NI-PR^{AVA} RT was more than NI-PR^{EMT} RT because of independency from the violation of $V_S/V_P = 0.5$ assumption. The estimation error could be decreased by either improving the AVO analysis or using a more reliable assumption about sedimentological parameters, especially porosity. It is the void space volume of sediments that control the effect of pore-filling substances on seismic responses; therefore an accurate assumption about the host sediment porosity is crucial in the RT analysis. This approach was also used for the BSR's NI-PR values, derived in five CRPs in different locations of thrusted-ridge, thrusted-footwall and basin-margin types of BSR in the Makran accretionary prism, offshore Iran. The quantification results near to BSR in the field data revealed lateral variations of hydrate and gas saturations between 4 to 30% and 1 to 7%, respectively, depending on the geological features such as dipping strata and

faults. For example, the presence of faults promoted the flux of free gas to the hydrate stability zone. This geologic event likely associated to formation of highly concentrated gas hydrate deposit where the saturation of free gas below the BSR is low.

ACKNOWLEDGMENTS

The Research and Technology Department of National Iranian Oil Company (NIOC) kindly sponsored this research. We are grateful to Geophysics Department of Exploration Directorate of NIOC for their kind consent to publish this work. We are also indebted to the associate editor and the reviewer for their valuable comments and suggestions.

REFERENCES

Athy, L.F., 1930. Density, porosity, and compaction of sedimentary rocks. AAPG Bull., 14: 1-24.

Castagna, J.P., Swan, H.W. and Foster, D.J., 1998. Framework for AVO gradient and intercept interpretation. Geophysics, 63: 948-956.

Dai, J., Xu, H., Snyder, F. and Dutta, N., 2004. Detection and estimation of gas hydrate using rock physics and seismic inversion: Example from northern deepwater Gulf of Mexico. The Leading Edge, 23: 61-66.

Domenico, S.N., 1976. Effect of brine-gas mixture on velocity in an unconsolidated sand reservoir. Geophysics, 41: 882-894.

Dvorkin, J. and Nur, A., 1993. Rock physics for characterization of gas hydrates: The Future of Energy Gases. U.S.G.S. Professional Paper, 1570, 293-298.

Dvorkin, J. and Nur, A., 1996. Elasticity of high porosity sandstones, Theory for two North Sea datasets. Geophysics, 61: 1363-1370.

Ecker, C., Dvorkin, J. and Nur, A., 1998. Sediment with gas hydrates: Internal structure from seismic AVO. Geophysics, 63: 1659-1669.

Fatti, J.L., Smith, G.C., Vail, P.J., Strauss, P.J. and Levitt, P.R., 1994. Detection of gas in sandstone reservoirs using AVO analysis: A 3-D seismic case history using the Geostack technique. Geophysics, 59: 1362-1376.

Fink, C.R. and Spence, G.D., 1999. Hydrate distribution off Vancouver Island from multifrequency single-channel seismic reflection data. J. Geophys. Res., 104: 2909-2922.

Fohrmann, M. and Pecher, I.A., 2012. Analysing sand-dominated channel systems for potential gas-hydrate-reservoirs using an AVO seismic inversion technique on the Southern Hikurangi Margin, New Zealand. Mar. Petrol. Geol., 38: 19-34.

Foster, D.J., Keys, R.G. and Lane, F.D., 2010. Interpretation of AVO anomalies. Geophysics, 75: A3-A13.

Fowler, S.R., White, R.S. and Louden, K.E., 1985. Sediment dewatering in the Makran accretionary prism. Earth Planet. Sc. Lett., 75: 427-438.

Gassmann, F., 1951. Elastic waves through a packing of spheres. Geophysics, 16: 673-685.

Hardage, B.A. and Roberts, H.H., 2006. Gas hydrate in the Gulf of Mexico: What and where is the seismic target?. The Leading Edge, 25: 566-571.

Hashin, Z. and Shtrikman, S., 1963. A variational approach to the elastic behavior of multiphase materials. J. Mech. Phys. Solids, 11: 127-140.

Helgerud, M.B., Dvorkin, J., Nur, A., Sakai, A. and Collett, T.S., 1999. Elastic wave velocity in marine sediments with gas hydrates: effective medium modeling. Geophys. Res. Lett., 26: 2021-2024.

Hosseini Shoar, B., Sedigh Arabani, M. and Javaherian, A., 2009. Application of seismic attributes for identification of gas hydrate bearing zone and free gas beneath it. Extended Abstr., 1st EAGE Conf., Shiraz: A36.

Hyndman, R.D. and Spence, G.D., 1992. A seismic study of methane hydrate marine bottom simulating reflectors. J. Geophys. Res., 97: 6683-6698.

Kennett, B.L.N., 1983. Seismic Wave Propagation in Stratified Media. Cambridge University Press, Cambridge.

Lin, C.C., Lin, A.T.S., Liu, C.S., Chen, G.Y., Liao, W.Z. and Schnurle, P., 2009. Geological controls on BSR occurrences in the incipient arc-continent collision zone off southwest Taiwan. Mar. Petrol. Geol., 26: 1118-1131.

Lu, S. and McMechan, G.A., 2004. Elastic impedance inversion of multichannel seismic data from unconsolidated sediments containing gas hydrate and free gas. Geophysics, 69: 164-179.

MacKay, M.E., Jarrard, R.D., Westbrook, G.K. and Hyndman, R.D., 1994. Origin of bottom simulating reflectors: geophysical evidence from the Cascadian accretionary prism. Geology, 22: 459-462.

Max, M.D., Johnson, A.H. and Dillon, W.P., 2006. Economic Geology of Natural Gas Hydrate. Springer Verlag, Dordrecht.

Mindlin, R.D., 1949. Compliance of elastic bodies in contact. J. Appl. Mech., 16: 259-268.

Minshull, T.A. and White, R.S., 1989. Sediment compaction and fluid migration in the Makran accretionary prism. J. Geophys. Res., 94: 7387-7402.

Muller, C., Bonnemann, C. and Neben, S., 2007. AVO study of a gas hydrate deposit, offshore Costa Rica. Geophys. Prosp., 55: 1-17.

Murphy, W.F.I., 1982. Effects of microstructure and pore fluids on the acoustic properties of granular sedimentary materials. Ph.D. thesis, Stanford University.

Ojha, M. and Sain, K., 2007. Seismic velocities and quantification of gas hydrates from AVA modeling in the western continental margin of India. Mar. Geophys. Res., 28: 101-107.

Ojha, M. and Sain, K., 2008. Appraisal of gas hydrates/free-gas from VP/VS ratio in the Makran accretionary prism. Mar. Petrol. Geol., 25: 637-644.

Ruppel, C., 2007. Tapping methane hydrates for unconventional natural gas. Elements, 3: 193-199.

Sain, K., Minshull, T.A., Singh, S.C. and Hobbs, R.W., 2000. Evidence for a thick free gas layer beneath the bottom simulating reflector in the Makran accretionary prism. Mar. Geol., 164: 3-12.

Sen, M.K., 2006. Seismic Inversion. Society of Petroleum Engineers, Texas.

Sheriff, R.E. and Geldart, L.P., 1995. Exploration Seismology. Cambridge University Press, New York.

Shuey, R.T., 1985. A simplification of Zoeppritz equations. Geophysics, 50: 609-614.

Sinha, B., Satyavani, N. and Thakur, N.K., 2004. Analysis of interval velocity vs amplitude blanking in a gas hydrate province. Curr. Sci., 87: 1605-1607.

Sloan, E.D., 1998. Clathrate Hydrate of Natural Gases. Taylor and Francis Group, New York.

Ursin, B., 1990. Offset-dependent geometrical spreading in layered medium. Geophysics, 55: 492-496.

Verm, R. and Hilterman, F., 1995. Lithology color-coded seismic sections: The calibration of AVO crossplotting to rock properties. The Leading Edge, 14: 847-853.

Walden, A.T., 1991. Making AVO sections more robust. Geophys. Prosp., 39: 915-942.

Warner, M., 1990. Absolute reflection coefficients from deep seismic reflections. Tectonophysics, 173: 15-23.

Wiggins, R., Kenny, G.S. and McClure, C.D., 1983. A method for determining and displaying the shear-velocity reflectivities of a geologic formation. European patent Application 0113944.

Yi, B.Y., Lee, G.H., Horozal, S., Yoo, D.G., Ryu, B.J., Kang, N.K., Lee, S.R. and Kim, H.J., 2011. Qualitative assessment of gas hydrate and gas concentrations from the AVO characteristics of the BSR in the Ulleung Basin, East Sea (Japan Sea). Mar. Petrol. Geol., 28: 1953-1966.

Zoeppritz, K., 1919. On the reflection and penetration of seismic waves through unstable layers. Erdbebenwellen VIIIB Göttinger Nachrichten, K1: 66-84.